Int J Adv Manuf Technol (2013) 67:1537–1548
DOI 10.1007/s00170-012-4588-z

ORIGINAL ARTICLE

Experimental observations on surface roughness, chip morphology, and tool wear behavior in machining Fe-based amorphous alloy overlay for remanufacture

Min Wang · Binshi Xu · Jiaying Zhang · Shiyun Dong · Shicheng Wei

Received: 8 June 2012 / Accepted: 24 October 2012 / Published online: 21 November 2012

Abstract Fe-based amorphous alloy, a new-type material, was developed as a special-purpose welt overlay for remanufacture. It was deposited on the worn-out part for resuming and upgrading part performance. The microstructure characteristics of the overlay was characterized, including microstructure, phase composition, thermostability, and microhardness. In order to get a comprehensive insight to the machining process of amorphous overlay, this paper presents an experimental investigation into the effect of various machining parameters and tool geometry (Edge) on the surface roughness, tool wear, chip morphology, and surface damage. Comparing larger rake angle of 15°and smaller nose radius of 0.4 mm with 5° and 0.8 mm at the same cutting parameters, we found that larger rake angle of 15° and smaller nose radius of 0.4 mm increased the R_a surface roughness parameter. In the tests, crater wear was not observed, and the friction and wear on the minor cutting edge wear were heavy due to the spring back of the machined surface. In brief, abrasion, adhesion, fatigue, and chipping are the main wear mechanism. As the feed rate reduced and the depth of cut increased (from feed rate=0.06 mm/rev and depth of cut= 0.3 mm to feed rate=0.09 mm/rev and depth of cut= 0.2 mm), a number of physical changes occurred in the chip including reduced distance between serrations, increased shear band angle, and changed chip morphology from spiral to ribbon shape. The results show that strain and strain rate rises in the chips' inside with the increase in cutting temperature. When the thermal softening exceeded strain hardening, the shear resistance decreased rapidly. Thus, the free surface of the chip presents the nodular and lamella structure. It was noted that specimens generated by larger rake angle of 15° and smaller nose radius of 0.4 mm showed poor surface roughness as well as extensive surface damage.

Keywords Remanufacturing technology · Fe-based amorphous alloy overlay · Tool wear mechanism · Chip formation mechanism

Highlights
▶Wear mechanism of tool and tribology characteristics of chip were revealed during cutting Fe-based amorphous alloy overlay.
▶A deformed shear band is due to severe plastic shear deformation in the chips of Fe-based amorphous alloy.
▶Surface roughness, tool failure, chip morphologies and the machined surface morphology of amorphous overlay at different cutting parameters were observed. And we found cutting speed is the main statistical significance on the surface roughness and surface damage.

M. Wang (✉)
School of Mechanical Engineering,
Beijing Institute of Technology,
Beijing 100081, People's Republic of China
e-mail: 10803016@bit.edu.cn

M. Wang · B. Xu · J. Zhang · S. Dong · S. Wei
National Key Laboratory for Remanufacture,
Beijing, 100072, People's Republic of China

M. Wang
TianDi Science and Technology Co,
Beijing 100013, People's Republic of China

1 Introduction and literature review

Remanufacturing technology has been used in practice for production of new parts with overlays, which have specific properties, and for renovation of the abraded, fatigued and fractured surfaces. In some cases, the use of suitable overlay can save materials and energy, optimize the part's performance, and expand the service life.

Today, remanufacturing technology has become a separate field of engineering and has developed rapidly in recent years. It is used in many different fields, e.g., metallurgy, traffic, petrochemistry, and other fields. Remanufacturing technology is also often employed in diesel engine and mining machinery due to the wear resistant overlays and corrosion resistant overlays.

In some cases, for remanufactured parts, it is possible to use the parts with an overlay without any additional finish, but sometimes, it is necessary to machine the remanufactured surface. Thus, the comprehension of the characteristics of Fe-based amorphous overlay in the process plays an important role in process optimization and surface integrity (roughness, residual stress, and surface texture) and thus part performance.

As a suitable hard coating material, TiAlN has been applied in cutting areas for a long time. TiAlN has a strong chemical stability and an antioxidation wear at 900 °C, and its hardness is 3400–3600 HV, which will translate into improving the abrasive resistance [1–3]. In this paper, TiAlN-coated tools were accepted as a comprehensive evaluation on surface roughness (R_a parameter) of the machined Fe-based overlay, tool wear behavior, and chip formation.

The mechanisms involved in the wear of cutting tools are rather complicated and may include different interacting effects linked together in a complex manner. Primarily, depending on cutting conditions, cutting parameters, work material, and tool material, the performance of the tool is limited by nose wear, flank wear, crater wear, edge chipping, or combination of these. Depending on the same parameters, the wear either occurs gradually by abrasive or adhesive wear, through plastic deformation, by more discrete losses of material through discrete fracture mechanism, or by combination of these [4].

Chip morphology is an important aspect in the cutting field, which is commonly considered to evaluate the machinability of products [5, 6] and explain the complex phenomena encountered in machining such as tool wear and surface integrity of the machined overlay.

Surface roughness (R_a parameter) of the machined surfaces is highly dependent on machining conditions, tool vibration, and chip effect [7], which influences the tolerance and fits of the components. The factor analysis of R_a parameter can reveal the influence of cutting parameters on tool wear and chip formation. Such study methods are referenced as following: Tuğrul Özel et al. [8] used a four-factor two-level factorial design (2^4) with 16 replications to determine the effects of the cutting tool edge geometry, work hardness, feed rate, and cutting speed on surface roughness and resultant forces in finish hard turning of AISI H13 steel using CBN tools. Furthermore, Tuğrul Özel and Karpat [9] developed predictive model of surface roughness and tool wear in hard turning using regression and neural network for AISI H13 using CBN tools. Bhushan et al. [10] made an attempt to systematically investigate the influence of cutting speed, depth of cut, and feed rate on surface roughness during machining of 7075 Al alloy and 10 wt% SiC particulate metal-matrix composites using tungsten carbide and polycrystalline diamond inserts.

Fe-based amorphous alloy, a new-type material, was developed as a special-purpose welt overlay for remanufacture. A comprehensive insight of its machining process has been a subject of research. Consequently, in this experimental work, the effect of tool geometry and machining parameters on the machined surfaces roughness, tool wear mechanisms, tool-chip tribological mechanisms, and chip morphology are selected to assess the machining process with PVD TiAlN-coated inserts.

2 Experimental details

2.1 Properties of Fe-based amorphous alloy overlay

Fe-based amorphous alloy (FeCrBSiNb) was deposited on the surfaces of worn out parts with a thickness of 1,200 μm, which was deposited on by wire arc spraying process. Fe-based cored wires (FeCrBSiNb) of 2 mm diameter were used as feedstock. The feedstock consists of conventional alloy powers, which contains specific atomic radios of elements to maximize glass. Medium carbon steel was used as the substrates. Prior to depositing, the substrates were degreased with acetone, dried in air, and grit-blasted. Then, the substrates were placed on a cylindrical fixture rotating around a vertical axis in front of the arc torch, which, in turn, traversed vertically. A self-designed wire arc gun system was employed for coating preparation by National Key Laboratory for remanufacture. The wire arc spraying parameters are as follows: spraying voltage, 36 V; spraying current, 120 A; compressed air pressure, 0.7 MP; and the stand-off distance was 200 mm.

The microstructures were characterized by scanning electron microscopy (SEM; Nova NanoSEM 460/650, FEI Co.), energy dispersive X-ray spectroscopy (EDS; Feature Max, OXFORD Co.), and transmission electron microscopy (TEM; Tecnai F20, Philips). The phase of the amorphous overlays was analyzed by XRD (Shimadzu, XRD700, Japan) using Cu Kα radiation (λ=1.5406 Å) produced by 40 kV and 30 mA. The analyzed range of the diffraction angle 2θ was between 20 and 80°, by a step width of 0.02°. The thermal stability and amorphous fraction of the amorphous overlay were examined by differential scanning calorimetry (DSC; NETZSCH, STA-449, Germany) in continuous heating mode at a rate of 10 K/s from room temperature to 1,000 K under nitrogen atmosphere. The microhardness value was calculated as average of 10 measurements recorded on polished cross-sections of the overlay under a 100 g load and 20 s loading time, using a HV-1000Z Vickers hardness tester.

The SEM image of the overlay is shown in Fig. 1. The overlay thickness is about 1,200 μm. From Fig. 1, it can be seen that the overlay is very dense, smooth, and few cracking. The overlay and the substrate are adhering well and compact.

Figure 2 shows the XRD pattern of the overlay. It can be seen that a broad halo peak appears at 2θ=44.77°, conforming

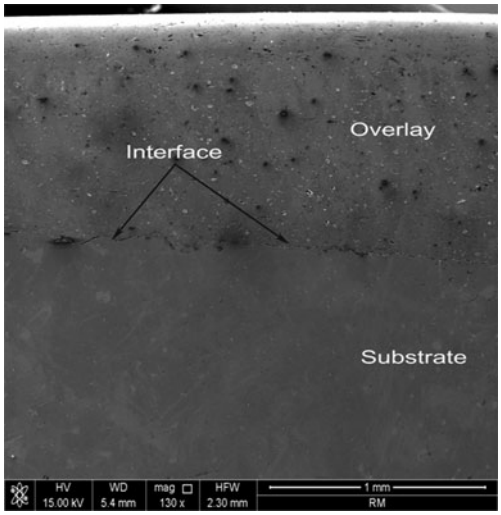

Fig. 1 SEM image of as-deposited overlay on the damaged parts

that an amorphous overlay was formed. The characteristic diffraction peak of α-(Fe, Cr) alloy indicates that nanocrystalline phases also exist in the overlay.

TEM was undertaken to obtain more detail information on microstructure formation of the overlay, as shown in Fig. 3. The diffused halo ring in selected area diffraction (SAEP) pattern sited at the right corner of micrograph confirms that the overlay is completely amorphous, in accordance with the XRD patterns given in Fig. 3a. As shown in Fig. 3b, fast Fourier transform (FFT), confirms the presence of mixture of nanocrystalline grains within an amorphous matrix. The microstructure of overlay consists of amorphous matrix embedding nanocrystalline particles ranging in size of 30–100 nm. The nanocrystalline grains were identified as bcc Fe-based in Fig. 3b.

To clarify the amorphous content of as-deposited remanufacturing overlay quantitatively, DSC curve was obtained at a heating rate of 10 K/min, as shown in Fig. 4. The DSC curve exhibits a sharp and strong exothermic peak, associated with rapid recrystallization of the amorphous during heating. The volume fraction of amorphous phase is

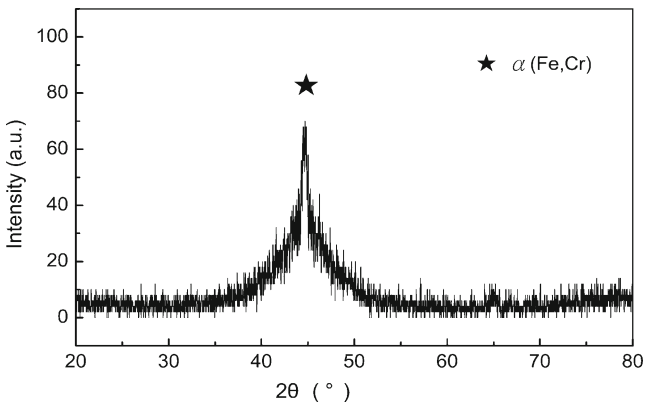

Fig. 2 XRD spectra of Fe-based amorphous alloy overlay

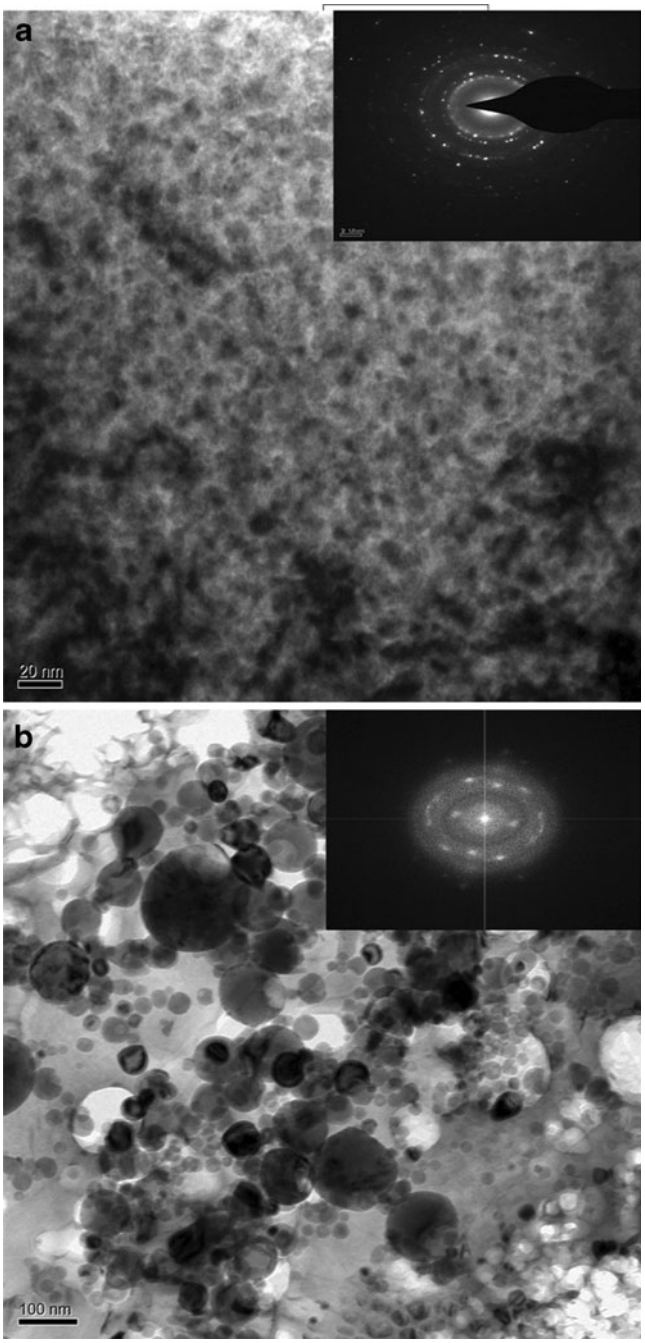

Fig. 3 TEM images of typical microstructure of the Fe-based amorphous alloy overlay including amorphous matrix and some nanocrystalline grains: **a** SAEP patterns showing a diffuse halo with diffraction spots and **b** FFT presenting a mixture of nanocrystalline grains, respectively

calculated by the crystallization enthalpy values (ΔH= −85.11–13.2 J/g=−98.31 J/g), which has been proved to be a fully amorphous structure by both previous work and other researcher [11]. In addition, the onset temperature of crystallization (T_x) is 531.4 and 812.2 °C, respectively. In other words, the amorphous overlay obtained with high thermal stability can be used in practice reliably and widely.

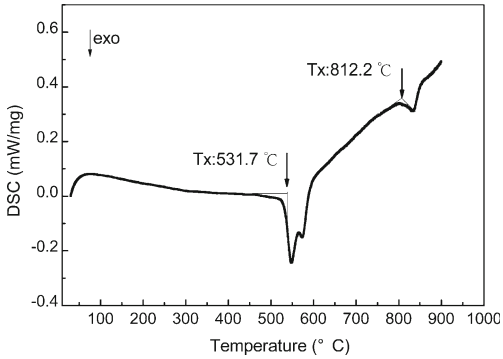

Fig. 4 DSC curve of Fe-based amorphous alloy overlay

Figure 5 shows the variation of microhardness across the interface from the substrate to the overlay. The microhardness was measured using a micro-Vickers tester (Jielun, HV-1000Z, shanghai, China). The Vickers hardness of the overlay is around $HV_{0.1}$=800–900 and is four times as the medium carbon steel.

X-ray photoelectron spectroscopy (XPS) analysis gives information not only on the bonding type of the atoms in solid phases but also on the composition and concentration of the components on the surface. With an ion-etching technique, it can also offer information on the inner surfaces. XPS spectra of element on Fe-based amorphous overlay after machining was obtained using ESCALAB 250Xi (Thermo Fisher Scientific, USA) with a monochromatic Al Kα X-ray source (1486.6 eV) operating at 15 kV. In the XPS analysis, the calibration of BE is the standard peak of adventitious C 1s (284.4 eV). Argon ions with 2 keV were used to etch the surface of the sample in order to remove the top contamination layer and to get the information on subsurface area of the overlay. In Fig. 6, XPS scan spectrum shows element aluminum and nitrogen permeated in Fe-based amorphous overlay after machining using TiAlN-coated inserts after removing the 4.8 nm top contaminations layer by ion etching.

The above theoretical analysis and experimental results prove that of amorphous alloy spraying coating was

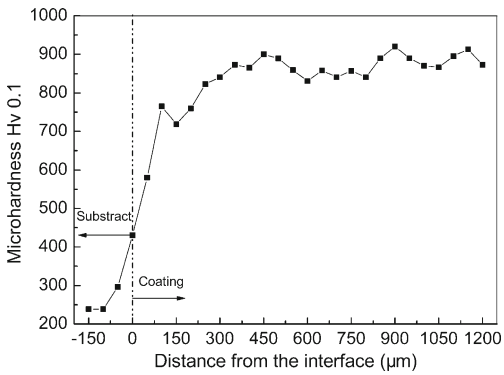

Fig. 5 Vickers hardness profile across the interface of the amorphous alloy overlay

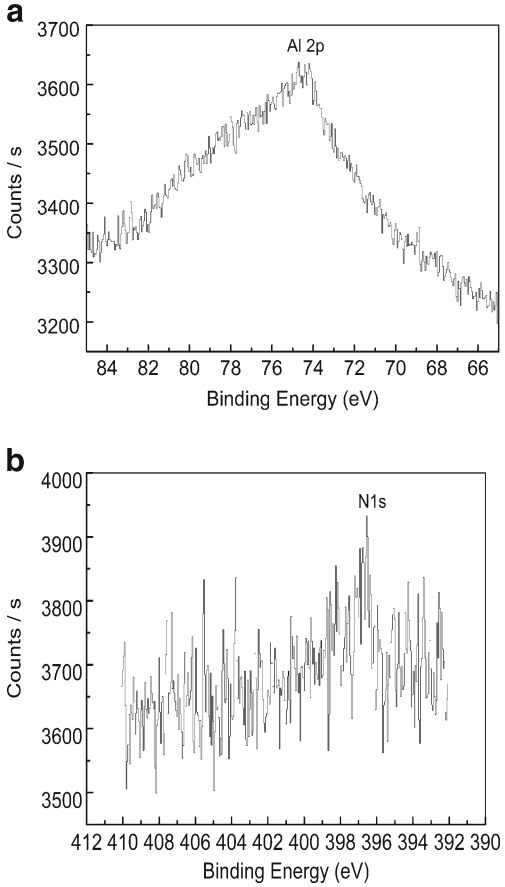

Fig. 6 XPS survey scan spectra of aluminum and nitrogen permeated Fe-based morphous overlay after machining using TiAlN coated tools **a** Al 2p pattern and **b** N 1s pattern

prepared by thermal spraying. Fe-based amorphous alloy was developed for repairing the damaged parts. The physics–mechanical properties for Fe-based amorphous alloy are better than the damaged parts of the same composition.

2.2 Properties of Fe-based amorphous alloy overlay

The chemical composition of the amorphous overlay used in this experiments includes 66.58 % Fe, 2.61 % Cr, 18.48 % B, 2.24 % Si, and 3.01 % Nb, which was deposited on the substrate of spoiled medium carbon steel. The thickness of the deposited overlay is 1.2 mm, and the substrate bars have a diameter of 44 mm. Therefore, the remanufactured parts have a diameter of 46.4 mm and a length of 160 mm.

In order to study the effect of cutting conditions and tool geometries on the surface roughness, tool wear, chip morphology, and surface damage, two types of PVD TiAlN-coated inserts are shown in Table 1. The inserts were all mounted on a right-hand tool holder “PCLNR2525M12” throughout the work separately, with major cutting edge angle of 95°, side cutting edge angle of 5°, and cutting edge inclinations angle of −6°.

Table 1 Properties of coated carbide tools

Type and factor	Tool I	Tool III
Coating method and material	PVD (TiAlN)	PVD (TiAlN)
Geometric form	CNMG120408-MP	CNMG120408-FP
Manufacturer and code	Kennametal KC5010	Kennametal KC5010
Rake angle	5°	15°
Nose radius	0.8 mm	0.4 mm

2.3 Experimental set-up and measuring instruments

CNC lathe of type "Millturn" by own design was employed to conduct the experiments. The CNC lathe is equipped with 5 kW spindle power and a maximum spindle speed of 2,000 rpm. A cylindrical bar is chucked with a three-jaw chuck at one end and supported by a live center at the tail stock. The workpiece chucking length was 154 mm.

Surface roughness R_a of machined surface was measured using the TIME TR240, a portable surface roughness measurement. The cut-off and sampling length for each measurement was taken as 0.8 and 2.5 mm, respectively. ISO 4287 standard specimen was followed during measurements. Three surface roughness measurements were made along the machined surface and an average of these values was taken as a response.

2.4 Design of experiment

A four-factor, two-level full factorial design was selected in this work to study the surface roughness so that all its interactions among independent variables and all its main effects can be investigated, though it was required to conduct large number of experiments. In this study, the four parameters namely cutting speed (V), feed rate (F), and tool geometry [rake angle (γ) and nose radius (R_ε)] were selected for the experimentation. The range of each parameter was set at two different levels. Based on a (2^4) full factorial design, a total of 22 unique experiments were carried out, which these factors and factor levels are summarized in Table 2.

Table 2 Factors and selected levels in turning experiments

Factor	Unit	Level	
		−1	1
V	m/min	60	80
F	mm/rev	0.06	0.12
DOC	mm	0.1	0.3
Edge		Tool 1I	Tool1III

3 Results and discussion

3.1 Surface roughness

An analysis of variance (ANOVA) was conducted to analyze the experimental results [12] and identify statistical trends to the surface roughness. Additionally, plots of significant factors corresponding to each AVONA analysis were constructed. These plots provide a more in-depth analysis of the significant factors related to the surface roughness in turning amorphous alloy overlay using different TiAlN-coated inserts. The method of least squares is used with the aid of MINITAB software.

3.1.1 ANOVA results

AVOVA tables for R_a surface roughness parameters are given in Table 3. In this study, the parameters with $p<0.05$ are considered to have a statistically significant contribution to the performance measure. Table 3 shows the main effects of Edge (Rake angle and nose radius) and interaction between feed rate and nose radius.

3.1.2 Effect of feed rate and tool geometry on surface roughness

Graphs of R_a surface roughness parameters are shown in Fig. 7. These figures have been constructed to illustrate the effects of interaction between feed rates and cutting speeds with variable Edge (rake angle and nose radius) on the surface roughness. It can be seen that surface roughness R_a decreases lightly with the interaction of cutting speeds, feed rate and variable Edge (e.g., rake angle, nose radius). Comparing larger rake angle of 15° and smaller nose radius of 0.4 mm with 5° and 0.8 mm at the same cutting parameters, we found that a larger rake angle of 15° and a smaller nose radius of 0.4 mm increases by 12 % of the R_a surface roughness parameter. This may be due to the fact that the larger rake angle increases cutting forces in agreement with our previous findings [13].

ANOVA results indicate that the effect of cutting speed as a single factor is no significant. This observation is in agreement with the findings of previous researchers [14]. However, it is pertinent to note that the main effects of interaction between feed rates and cutting speeds with variable tool geometry (e.g., effective rake angle and nose radius) are significant to surface roughness.

3.2 Tool wear mechanisms

The common wear mechanisms are adhesive, diffusion, oxidation, and chipping, so as to the wear in the machining process for TiAlN-coated tool. The TiAlN coating reduces

Table 3 Analysis of variance for R_a surface roughness after removing insignificant terms

Term	Coefficient	SE coefficient	T	P value		
Constant	0.9144	0.01741	52.52	0.000		
F	−0.0402	0.02042	−1.97	0.040		
γ	0.0544	0.01741	3.13	0.017		
R_ε	−0.0741	0.02042	−3.63	0.008		
$V\times F$	−0.0501	0.02042	−2.45	0.044		
$V\times\gamma$	0.0958	0.02042	4.69	0.002		
$V\times R_\varepsilon$	0.1363	0.02042	6.68	0.000		
$F\times R_\varepsilon$	−0.1116	0.02042	−5.46	0.001		
$\gamma\times R_\varepsilon$	−0.1582	0.02042	−7.75	0.000		
$V\times F\times\gamma$	0.1293	0.02042	6.33	0.000		
$V\times F\times R_\varepsilon$	0.0623	0.02042	3.05	0.019		
$F\times\gamma\times R_\varepsilon$	−0.1417	0.02042	−6.94	0.000		
S=0.0816625		PRESS=1.04771				
R^2=97.63 %		R^2(adj)=92.90 %				
Source	*df*	Seq SS	Adj SS	Adj MS	F	P value
Main effects	4	0.19002	0.19002	0.047505	7.12	0.013
Two-way interactions	6	1.08486	0.180810	0.180068	27.11	0.000
Three-way interactions	4	0.65118	0.65118	0.162794	24.41	0.000
Residual error	7	0.04668	0.04668	0.006669		
Curvature	1	0.02442	0.02442	0.024423	6.58	0.043
Lack of fit	2	0.00913	0.00913	0.004563	1.39	0.348
Pure error	4	0.01313	0.01313	0.003283		
Total	21	1.97274				

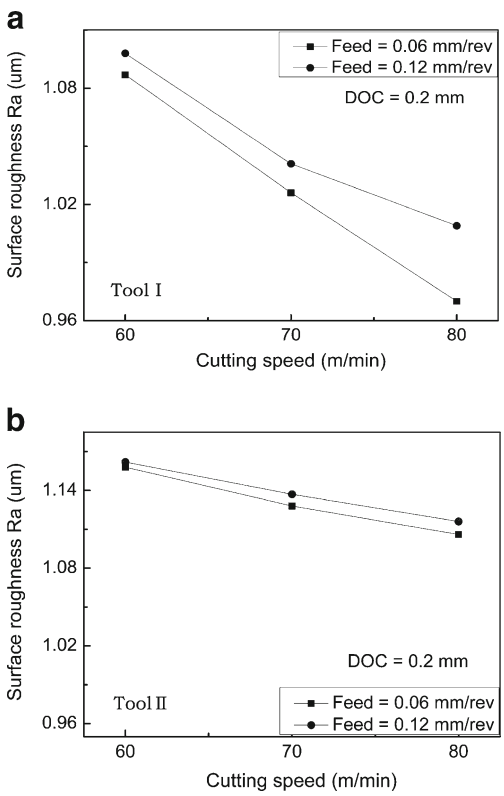

Fig. 7 Influence of cutting speed and feed on the surface roughness at constant depth of cut of 0.2 mm using different TiAlN coated tools

friction between the tool and workpiece owing to its low friction coefficient and prevents the oxidation of the solid carbide or other erosions. In addition, Al_2O_3 produced by oxidation reaction of presence Al in the coating dramatically improves the wear resistance to prolong the cutting life [1].

To illustrate the failure modes of the tools under different cutting conditions, in this paper, the flank was separated into two components, the flat primary flank on the leading edge and the curved flank on the tip of the inserts (i.e., the nose) [15].

At the first test interrupt, the abrasive wear along the flank was observed at 60 m/min in constant feed cuts (F= 0.06 mm/rev, DOC=0.2 mm). As shown in Fig. 8 (a-b), deep grooves were parallel to the direction of workpiece rotation resulting from rubbing of flank face with overlay surface during turning. Subsequently, with increasing of feed rate as well as depth of cut (F=0.12 mm/rev, DOC= 0.2 mm), a built-up edge (BUE) was also observed along the rake face in Fig. 8c, which means that adhesive wear has occurred. Adhesive wear can be testified through analyzing the place D by EDS (Fig. 9b).The material of particle D marked in Fig. 9a consists of 49.16 wt% of Fe and 0.71 wt% of Si all of which come from Fe-based overlay. Because of the coupling action from the high temperature and pressure, the plastic deformation and cold welding occur at the

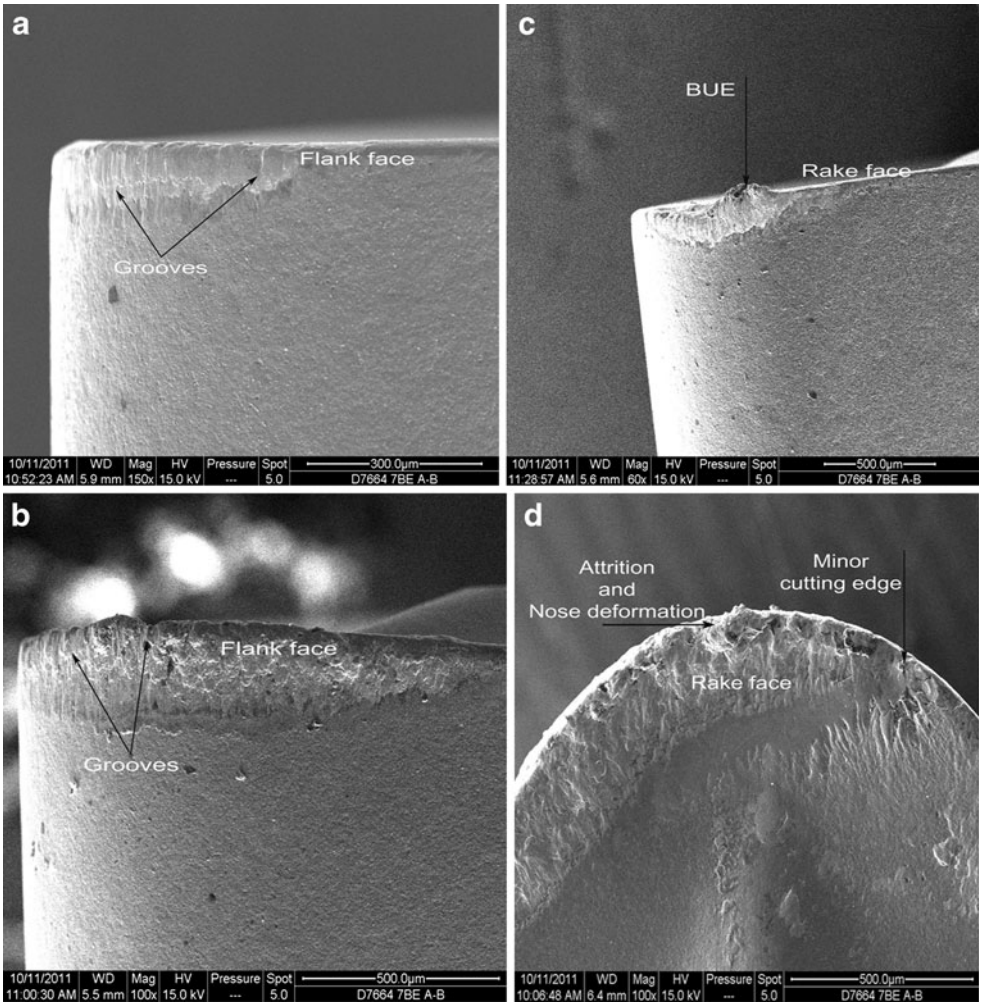

Fig. 8 SEM images of TiAlN coated insert wear under various cutting conditions: **a** V=60 m/min, F=0.06 mm/rev, DOC=0.2 mm; **b** V=60 m/min, F=0.12 mm/rev, DOC=0.2 mm; **c** V=70 m/min, F=0.09 mm/rev, DOC=0.2 mm; **d** V=70 m/min, F=0.12 mm/rev, DOC=0.2 mm

interface between tool and overlay to produce the atomic absorption. With high stress and the relative motion at the interface, the Fe enriched in the amorphous overlay is easy to adhere to the tool surface and to be teared off or removed from the overlay [16].

When the cutting speed increased beyond 70 m/min in constant feed cuts (F=0.09 mm/rev and DOC=0.2 mm), the high temperature brings another phenomenon that chemical affinity was found from the tool to the amorphous overlay. The X-ray photoelectron spectroscopic analysis (Fig. 6) shows that aluminum and nitrogen have permeated into the surface of overlay. This is the chemical wear, which changed the compositions of Fe-based overlay surface through the interdiffusion of TiAlN-coating elements between tool and Fe-based overlay. It is the most important wear mechanism in the catastrophic stage, and it gives a message that the carbide substrate is exposed, as the result the TiAlN coating are snatched from the tool to form diffusive wear. Further cutting increased the extent of cracks and factures and accelerated the fatigue wear, shown in Fig. 8d. The cycle heating and cooling and the fluctuation of the mechanical loading generated the alternate stress composing the thermal and mechanical stresses in the machining process [1]. The cracks and plastic deformations distributed parallel to the cutting edge under the combined effects by dynamic stress. However, the propagating cracks render small chips easily break off from the cutting edge especially when irregular shear fracture of chips and partial breakage of BUE. Figure 9 shows that microchipping were appeared at the cutting edge, which means that fatigue had occurred, and subsequently, the tool failed.

3.3 Chip formation mechanisms

In the machining process, chip formation directly affects the machining behavior such as cutting temperature, surface roughness, tool wear, etc. [17, 18]. The chips were collected during the cutting tests for studying their nature of formation under different cutting parameters when machining Fe-based amorphous alloy.

The SEM micrographs reveal that the shape of chip presents ribbon and spiral shape as shown illustratively in Fig. 10a and b. As the feed rate reduced and the depth of cut increased, a number of physical changes occurred in the

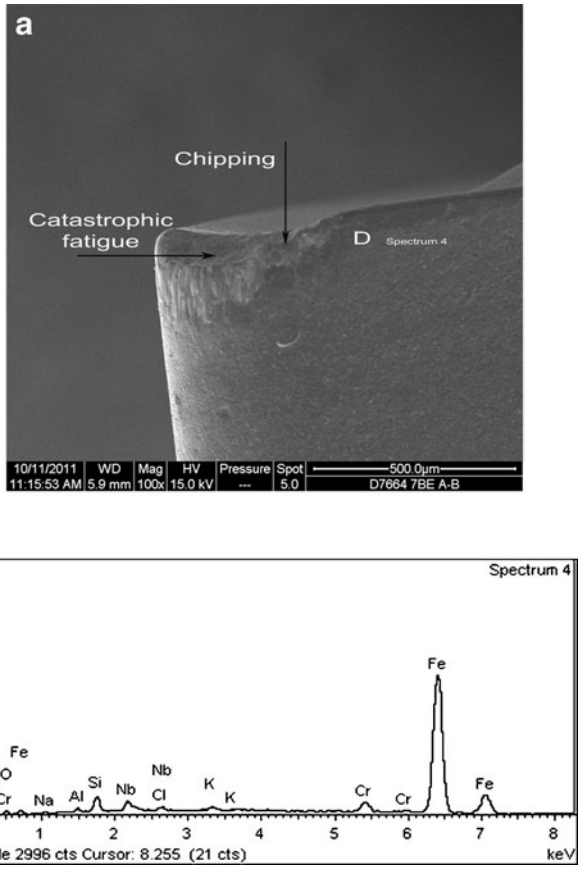

Fig. 9 **a** SEM micrograph of the chipping and catastrophic fatigue on the cutting edge at V=80 mm/min, F=0.12 mm/rev, DOC=0.3 mm. **b** EDS spectrum of the particle D marked in **a**

chip including reduced distance between serrations and increased shear band angle (measuring technique reported elsewhere [20]) in Fig. 11a and b. The parameter about the spiral shape of chips could be represented as:

$$\tan\theta = \frac{\rho_x}{\rho_z \cos\eta} \tag{1}$$

$$d = 2\sqrt{\frac{1-\sin^2\eta\cos^2\theta}{(\cos\eta/\rho_x)^2(1/\rho_z)^2}} \tag{2}$$

where θ reflect the angle between spiral and the axis, d is the spiral diameter, $1/\rho_x$ is the crimp chip curvature, $1/\rho_z$ is the horizontal chip curvature, and η is the chip flow angle [19], as shown in Fig. 10c. Observing the morphology changes between the free surface and back surface, the free surface of the chip has loose and lamella structure, as shown in Fig. 11a and b, and then, the back surface of the chip is more uneven and rough. Some grooves have been found on the back surface of the chip, which responds to the wear failure of the cutting edge. In the EDX spectrometry in Fig. 11c, we can find Fe, Cr, B, and O elements. Perhaps, transfer film of

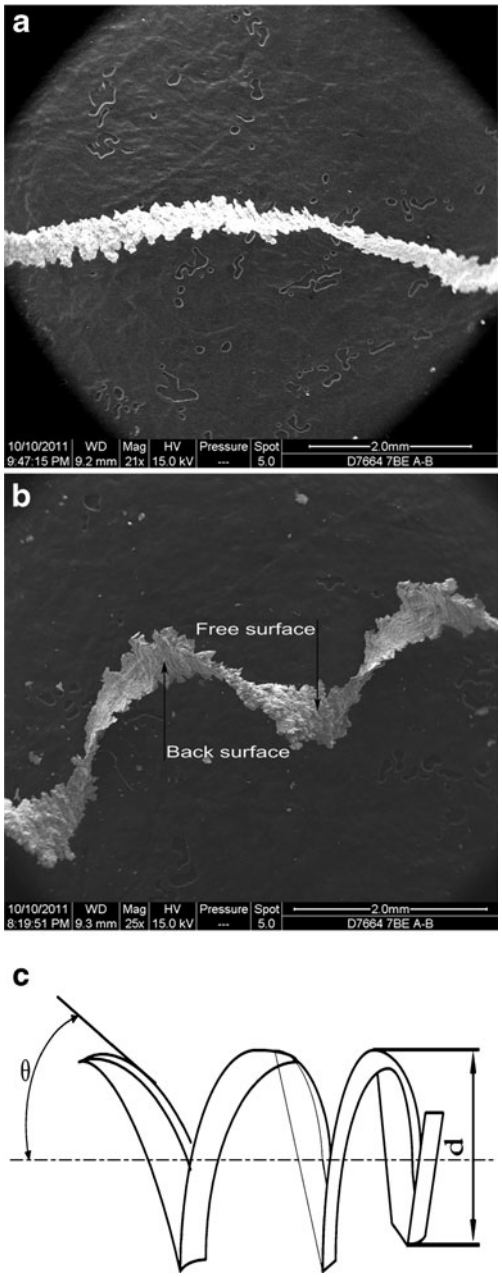

Fig. 10 SEM imagines of chips obtained at various cutting conditions: **a** V=70 m/min, F=0.09 mm/rev, DOC=0.2 mm; **b** V=70 m/min, F=0.12 mm/rev, DOC=0.2 mm; **c** schematic diagram of chip with some parameters

B_2O_3 and Al_2O_3 was formed on the cutting tool. The chemical reaction can occur as follows:

$$4Al + 3O_2 \rightarrow 2Al_2O_3 \tag{3}$$

$$4B + 3O_2 \rightarrow 2B_2O_3 \tag{4}$$

In the initial wear stage between chip and tool, chips can flow smoothly out from rake face without impeding, since the rake face is protected by TiAlN coating and the cutting

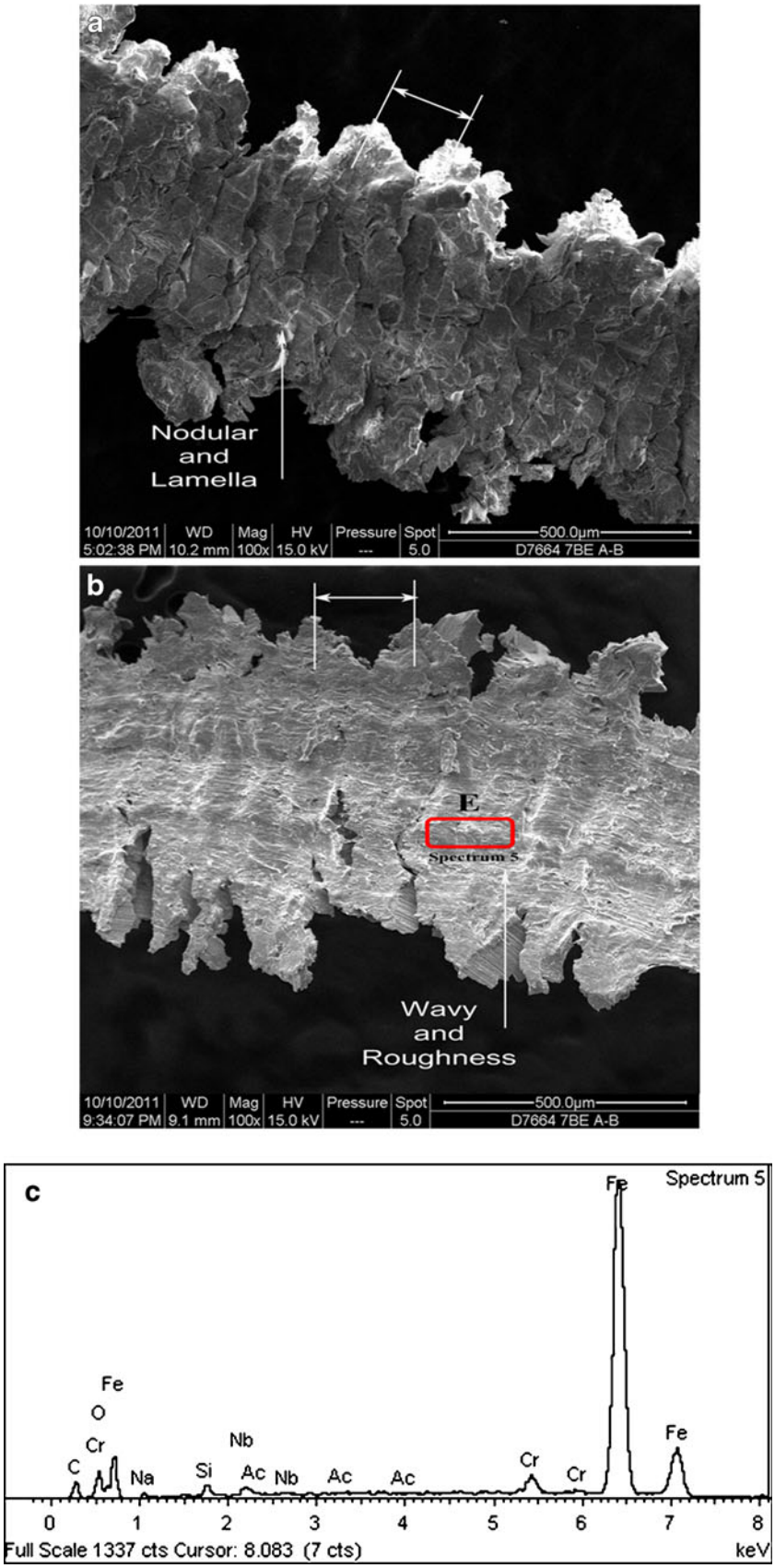

Fig. 11 Micrographs of serrated chips obtained at cutting conditions in gradual wear stage: **a** V=60 m/min, F=0.06 mm/rev, DOC=0.2 mm; **b** V=70 m/min, F=0.12 mm/rev, DOC=0.2 mm; **c** EDS analysis of zone E

edge is integrity and tartness. Moreover, the cutting force is low, and the plastic deform that effected chip morphology during cutting process is minimum in this wear stage[21]. Therefore, the back of the chips are smooth and even. With cutting quantity increasing, the cutting edge is becoming blunt and dull to cause the tearing action during the cutting process; as a result, a roughness back surface with burrs emerged. However, the plastic formation of back surface is constrained by the tool rake face. Thus, the back face experiences the high contact pressure and frictional force when the chip slides over the tool rake face. The combined actions of high contact pressures, frictional forces, and high temperatures form the back surface [22]. With the continuity of cutting, the friction between the chip and rake face causes the generation of chip temperature [23]. The results show that strain and strain rate rises in the chips' inside with the increase in cutting temperature. When the thermal softening exceeded strain hardening, the shear resistance decreased rapidly. Thus, the free surface of the chip presents the nodular and lamella structure, as shown in Fig. 11a. Thereby, the back face of chip easily adheres to the rake face under high friction and the chip flowing are impeded. Consequently, uneven back surface appears with grooves and voids, as shown in Fig. 11b.

3.4 Surface damage analysis

Usually, possible surface alterations that occur in conventional metal-removal processes depend on the workpiece material grade. The alterations include the following alterations: plastic deformation, built-up-edge, laps and tears, crevice-like defects, burrs, and microcracks.

Nevertheless, for Fe-based amorphous alloy overlay, reinforced grains scattered in amorphous overlay (shown in Fig. 12a) improve the performance of the overlay and worsen the machined surface morphology because particle fracture and displacement occurs in machining. SEM was used to examine the machined surface of amorphous overlay and assess the effect of machining parameters and tool geometry on machined surface damage.

At lower cutting speed (i.e., 60 m/min), a BUE was observed along the rake face (as shown in Fig. 8c). Due to built-up-edge formation, irregular type of machined surface was observed including feed marks, plastic deformation,

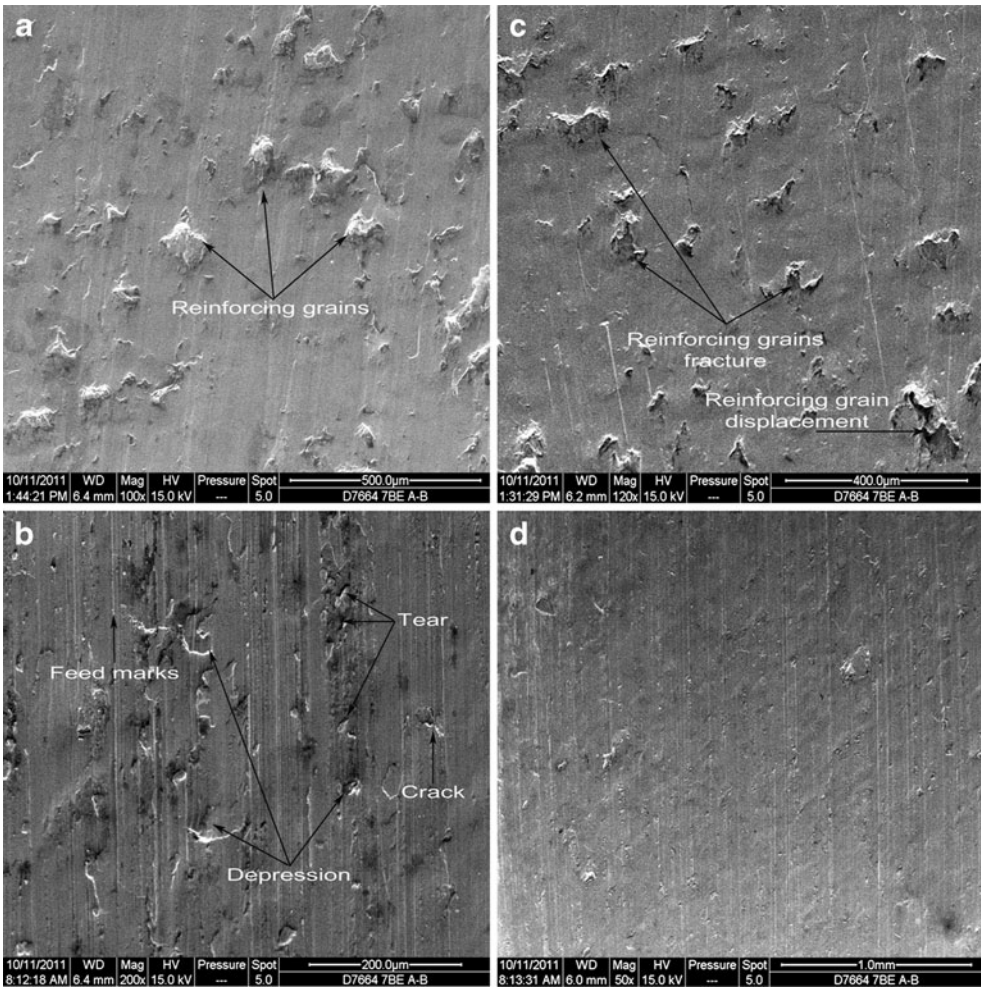

Fig. 12 SEM micrographs of **a** overlay surface of amorphous alloy, **b** machined surface generated by BUE at V=60 m/min, **c** machined surface generated by ploughing at V=70 m/min, and **d** smooth and even surface generated by at V=80 m/min

tearing, cracking, etc., as shown in Fig. 12b. A BUE deposit was a form of lap and as such was an addition to overlay surface. Often a crack was formed below the BUE on the machined surface. This crack and crevice-like defect can be highly detrimental to the fatigue strength of the material. Tears occurred because the adhesion between the tool and the overlay surface was so high as to tear away some parts of the surface. As a result, a depression (called the worn-out) in the surface occurred, causing the surface topography to be disturbed. When cutting speed beyond 70 m/min under different feed rates and depths of cut, fracture, and displacement of reinforcing particles (seen in Fig. 12c) were found because plowing effect prevailed at smaller depth of cut (0.1 mm) and lower feed rate (0.06 mm/rev). Whereas the machined surface (seen in Fig. 12d) at higher cutting speed (i.e., 80 m/min) and lower depth of cut (0.1 mm) showed less surface damage due to thermal softening produced by increasing the cutting speed compared with the surfaces generated by cutting speeds of 60 and 70 m/min. As the depth of cut increased, the machined overlay became worsened for the reason that the effect of the machining forces exceeded the softening speed of machined overlay influenced by the increased cutting speed [24].

In short, Fe-based amorphous alloy can be applied in the remanufacturing of the damaged parts. The material has better mechanical prepared on the surface of the damaged parts. However, mechanical machining of the coating is the key to development of industrialization of remanufacturing technology, which contains tool life and working efficiency, on which is research based for remanufacturing technology.

4 Conclusions

Based on test results of the various set of experiments in Fe-based amorphous alloy overlay, the influence of cutting parameters on the surface roughness, tool wear, chip morphology, and surface damage was analyzed. The following conclusions are drawn:

- The statistical analysis of the experimental results shows that the larger effective rake angle and smaller nose radius(15° and 0.4 mm) increases surface roughness R_a, comparing with using ToolI (5° and 0.8 mm). Interaction of cutting speed, feed rate, and effective rake angle, and interaction of feed rate, effective rake angle, and nose radius are the most significant with respective to surface roughness parameter R_a.
- The optimal machining conditions for machined amorphous overlay surface quality using PVD TiAlN-coated inserts were identified as V=80 m/min, F=0.09 mm/rev, DOC=0.1 mm, TiAlN-coated tool (γ=5° and R_ε= 0.8 mm).
- Abrasion, adhesion, and fatigue are the main wear mechanism at different cutting parameters. The chemical dissolution type of wear is slightly observed due to existing BUE. Tool failure modes were flank wear, plastic lowering at minor edge, and catastrophic chipping at the tool nose.
- The chip presents ribbon and spiral shape. The chip morphology of the free surface in the initial stage is smooth and even; in the semisteady stage, the back surface of chips are wavy and rough due to the tearing cutting. The formation mechanism of the difference morphology is due to the combined actions of high contact pressures, frictional force, and high temperatures.

References

1. Wang YG, Yan XP, Li B, Tu GC (2012) The study on the chip formation and wear behavior for drilling forged steel S48CS1V with TiAlN-coated gun drill. Int J Ref Met Hard Mat 30(1):200–207
2. Gill SS, Singh J, Singh H, Singh R (2011) Investigation on wear behaviour of cryogenically treated TiAlN coated tungsten carbide inserts in turning. Int J Mach Tools Manuf 51(1):25–33
3. Castanho JM, Vieira MT (2003) Effect of ductile layers in mechanical behavior of TiAlN thin coatings. J Mater Process Technol 143–144(20):352–357
4. Hogmark S, Olsson M (2005) Wear mechanisms of HSS cutting tools. SME Tech Paper 1:1–14
5. Venkatesh VC, Zhou DQ, Xue W, Quinto DT (1993) A study of chip surface characteristics during the machining of steel. Ann CIRP-Manuf Technol 42(1):631–636
6. Lorentzon J, Järvstråt N, Josefson BL (2009) Modelling chip formation of alloy 718. J Mater Process Technol 209(10):4645–4653
7. Töenshoff HK, Arendt C, Amor RB (2000) Cutting hardened steel. Ann CIRP Manuf Technol 49:547–566
8. Özel T, Hsu HK, Zeren E (2005) Effects of cutting edge geometry, workpiece hardness, feed rate and cutting speed on surface roughness and forces in finish turning of hardened AISI H13 steel. Int J Adv Manuf Technol 25(3–4):262–269
9. Özel T, Karpat Y (2005) Predictive modeling of surface roughness and tool wear in hard turning using regression and neural networks. Int J Mach Tools Manuf 45(4–5):467–497
10. Bhushan RK, Kumar S, Das S (2010) Effect of machining parameters on surface roughness and tool wear for 7075 Al alloy SiC composite. Int J Adv Manuf Technol 50(5–8):459–469
11. Ponnambalam V, Poon SJ, Gary JS (2004) Fe-Based bulk metallic glasses with diameter thickness larger than one centimeter. J Mater Res 19:1320–1323
12. Thiele JD, Melkote SN (1999) Effect of cutting edge geometry and workpiece hardness on surface generation in the finish hard turning of AISI 52100 steel. J Mater Process Technol 94(2–3):216–226
13. Singh D, Rao PV (2007) A surface roughness prediction model for hard turning process. Int J Adv Manuf Technol 32(11–12):1115–1124
14. EL-Wardany TI, Kishawy HA, Elbestawi MA (2000) Surface integrity of die material in high speed hard machining. Part 2: microhardness variation and residual stress. Trans ASME-J Manuf Sci Eng 122(11):632–641

15. Bermingham MJ, Kirsch J, Sun S, Palanisamy S, Dargusch MS (2011) New observation on tool life, cutting forces and chip morphology in cryogenic machining Ti-6Al-4V. Int J Mach Tools Manuf 51(6):500–511
16. Lin KL, Chao WH, Wu CD (1997) The performation and degradation behavior of the TiAlN/interlayer coating on the drill. Surf Coat Technol 87(3):274–284
17. Simoneau A, Ng E, Elbestawi MA (2006) The effect of microstructure on chip formation and surface defects in microscale, mesoscale, and macroscale cutting of steel. Ann CIRP 55(1):97–102
18. Monaghan J, Brazil D (1998) Modelling the flow processes of a particle reinforced metal matrix composite during machining. Compos A: Appl Sci Manuf 29(1–2):87–99
19. Nakayama K, Ogawa M (1978) Basic rules on the form of chip in metal cutting. Ann CIRP 27(1):17–20
20. Sun S, Brandt M, Dargusch MS (2009) Characteristics of cutting forces and chip formation in machining of titanium alloys. Int J Mach Tools Manuf 49(7–8):561–568
21. Aykut S, Bagci E, Kentli A, Yazlcloglu O (2007) Experimental observation of tool wear, cutting forces and chip morphology in face milling of cobalt based super-alloy with physical vapour deposition coated and uncoated tool. Mater Des 28(6):1880–1888
22. Hou ZB, Komanduri R (1997) Modeling of thermomechanical shear instability in machining. Int J Mech Sci 39(11):1273–1314
23. Li B (2011) Chip morphology of normalized steel when machining in different atmospheres with ceramic composite tool. Int J Ref Met Hard Mater 29(3):384–391
24. Gaitonde VN, Karnik SR, Figueira L, Davim JP (2009) Machinability investigations in hard turning of AISI D2 cold work tool steel with conventional and wiper ceramic inserts. Int J Ref Met Hard Mat 27(4):754–763